Available online at www.sciencedirect.com
SCIENCE DIRECT®
Carbohydrate Research 338 (2003) 2311–2324
CARBOHYDRATE RESEARCH
www.elsevier.com/locate/carres

Electrospray tandem mass-spectrometric analysis of diastereo- and stereoisomeric pyrimidine nucleoside analogues based on the 1,3-dihydrobenzo[*c*]furan core

Christophe Len,[a] Grahame Mackenzie,[b] David F. Ewing,[b] George Sheppard,[c] Joseph Banoub[c,d,*]

[a] *Laboratoire des Glucides, Université de Picardie-Jules Verne, F-80039 Amiens, France*
[b] *Department of Chemistry, University of Hull, Hull HU6 7RX, UK*
[c] *Department of Fisheries and Oceans, Science Oceans and Environment Branch, St. John's, NL, Canada A1C 5X1*
[d] *Biochemistry Department, Memorial University, St. John's, NL, Canada A1C 5S7*

Received 16 May 2003; accepted 29 August 2003

The authors dedicate this paper to Professor Hassan El Khadem on the occasion of his 80th birthday

Abstract

Electrospray mass spectrometry and tandem mass spectrometry have aided the structural characterization of the diastereoisomeric *cis*- and *trans*-1-(3-benzoyloxymethyl-1,3-dihydrobenzo[*c*]furan-1-yl)thymines and the four enantiomerically pure stereoisomers of uracil analogues. Low-energy collision-induced dissociation MS/MS analysis of the various precursor molecular and cluster ions confirmed the characteristic fingerprint pattern obtained in the conventional electrospray spectra and allowed a convenient method for the characterization of novel 1,3-dihydrobenzo[*c*]furan nucleosides.

Keywords: Structural characterization; Electrospray tandem mass spectrometry; Thymine diastereoisomers; Uracil enantiomers of 1,3-dihydrobenzo[*c*]furan nucleosides

1. Introduction

In the search for novel antiviral agents for the treatment of Acquired ImmunoDeficiency Syndrome (AIDS), competitive nucleoside inhibitors of the retroviral reverse transcriptase (RT) continue to be one of the most promising classes of compounds. Nucleosides approved by the US Food and Drug Administration for the treatment of the Human Immunodeficiency Virus (HIV) are zidovudine (AZT, Retrovir),[1] zalcitabine (ddC, Hivid),[2] didanosine (ddI, Videx),[3] lamivudine (3TC, Epivir),[4] abacavir (ABC, 159U89, Ziagen),[5] and stavudine (d4T, Zerit).[6] D4T shows selective anti-HIV activity comparable to that of AZT in vitro and is less toxic and less inhibitory to mitochondrial DNA replication than AZT[7] (Scheme 1). One disadvantage of d4T is the facile cleavage of the glycosidic bond by a specific phosphorylase. Much effort and interest by a number of laboratories have been directed towards the synthesis of d4T analogues with improved stability and which do not stimulate viral mutations.

Nucleoside analogues with conformational rigidity imposed by locking the conformation of the furanose (or carbocyclic) ring by introducing a second ring are now of great interest. Several nucleosides with a bicyclic glycone have been synthesized in the search for conformationally restricted systems which might lead to enhanced duplex formation when incorporated into oligonucleotides. Mackenzie's group has developed an asymmetric synthesis of d4T analogues based on a 1,3-dihydrobenzo[*c*]furan glycon core.[8–11] This new type of nucleoside analogue is important for several reasons: (i) the enhanced phosphorylation due to the presence of the phenyl group as has been observed in some imidazole

* Corresponding author.
E-mail address: banoubjo@dfo-mpo.gc.ca (J. Banoub).

0008-6215/03/$ - see front matter.
doi:10.1016/j.carres.2003.08.017

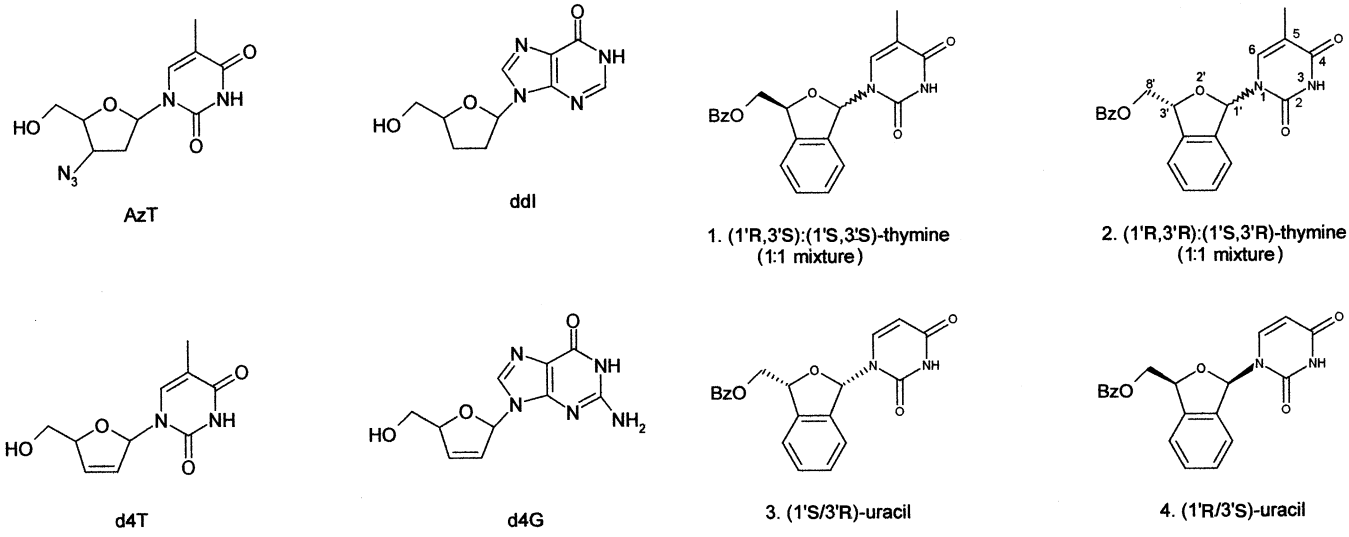

Scheme 1.

Scheme 2.

nucleosides;[12] (ii) the increased stability of the glycosidic bond due to the presence of the aromatic ring; (iii) the improved membrane transport due to the increased lipophilicity; (iv) the enhanced rigidity of the system. Efficient routes for the synthesis of uracil, thymine, and cytosine derivatives of 1,3-dihydrobenzo[*c*]furan, which are aromatic analogues of the well known antiviral 2′,3′-dideoxy-2′,3′-didehydronucleosides, have been described.[8–14] These systems contain two chiral centers, (C-1′ and C-3′, as shown in Scheme 2) corresponding to the α/β and D/L centers in a furanose sugar. The asymmetric synthesis protocol used in our work[10] provides compounds which are stereochemically pure at the C-3′ site and a 1:1 mixture of both stereoisomers at the C-1′ site. Final resolution of each pair of diastereoisomers is easily achieved chromatographically to afford the four enantiomerically pure enantiomers.[10] In this work we investigate the thymine derivatives as the two diastereoisomeric mixtures, **1** (1′*R*,3′*S*) with (1′*S*,3′*S*), and **2** (1′*R*,3′*R*) with (1′*S*,3′*R*). The analogous uracil compounds were available as the four optically pure stereoisomers (1′*S*,3′*R*) **3**, (1′*R*,3′*S*) **4**, (1′*S*,3′*S*) **5**, and(1′*R*,3′*R*) **6**.

To our knowledge, there have been no previous studies on the mass-spectrometric characterization of this novel series of pyrimidine nucleoside analogues based on the 1,3-dihydrobenzo[*c*]furan core. As a continuation of our interest in the mass-spectrometric studies and tandem mass-spectrometric differentiation of anomeric and regioisomeric 2′-deoxyribofuranosyl imidazole nucleosides,[14–16] amphiphilic regioisomeric esters of sucrose,[17,18] anomeric pairs of 3′-azido-2′,3′,4′-trideoxy-4′-thio(halo)uridine series of diastereoisomeric 1,2-*trans*-2-deoxy-2-iodoglycosyl azides,[19,20] and other bioactive carbohydrate molecules,[21–25] we now report the ESIMS and low-energy collision induced dissociation tandem mass spectra (CID MS/MS) of the series of compounds of **1**–**6**.

With access to four pure stereoisomers of the uracil analogues **3**–**6** it was possible to investigate the way stereochemistry could affect the structural information

Table 1
Electrospray mass spectra of diastereomeric mixtures of *cis*- and *trans*1-(3-benzoyloxymethyl-1,3-dihydrobenzo[*c*]furan-1-yl)thymines (**1** and **2**) recorded with a cone voltage of 20 V

Compounds	Characteristic ions						
		$[2M+Na]^+$	$[2M+H]^+$	$[M+Na]^+$	$[M+H]^+$	[S]	$[S-C_6H_5Co_2H]^+$
	m/z	779	757	401	379	253	131
(1′*R*,3′*S*),(1′*S*,3′*S*) **1**	%	23	48.2	23	61.8	74.2	100
(1′*R*,3′*R*),(1′*S*,3′*R*) **2**	%	13	39.6	20	26.7	69	100

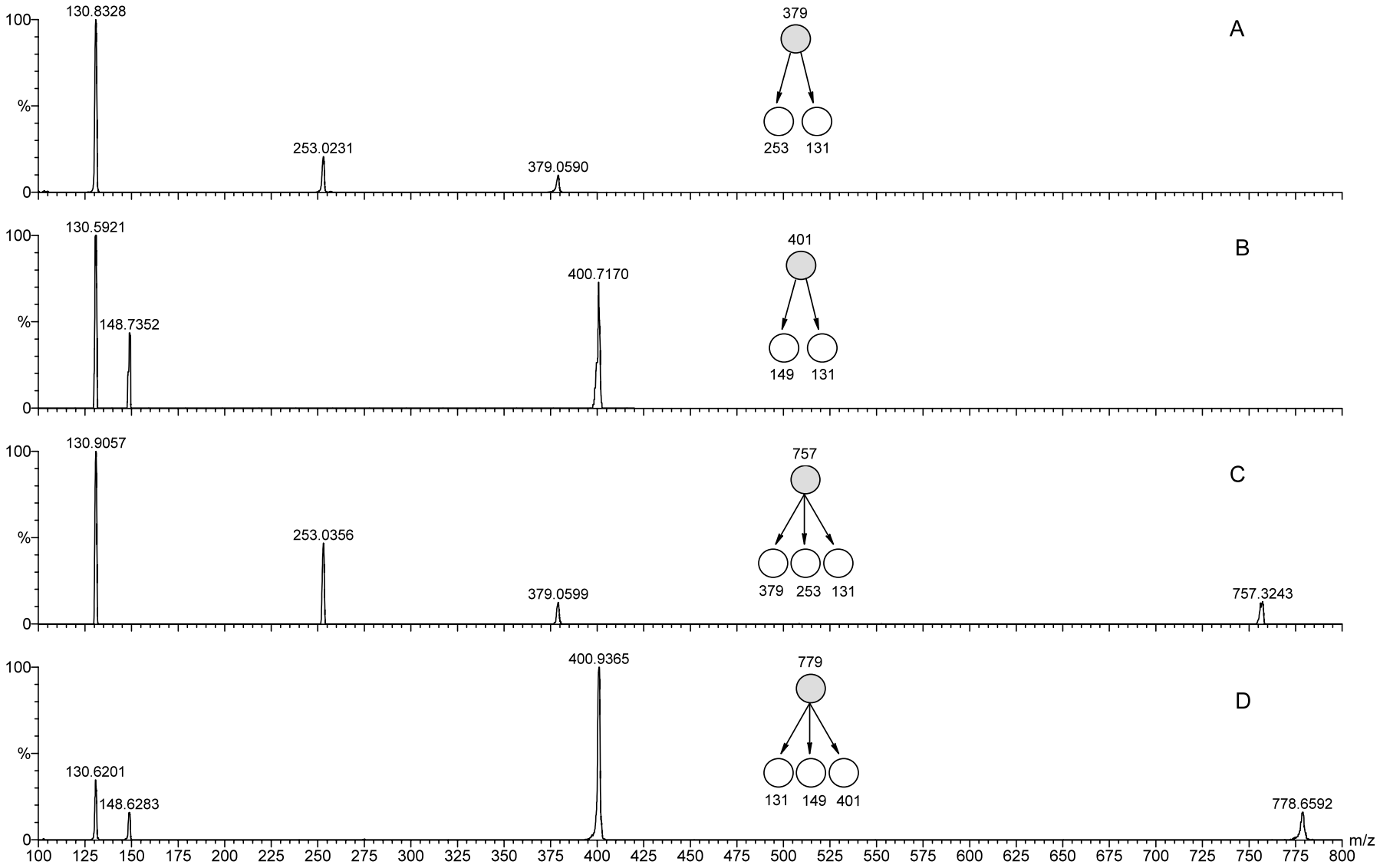

Fig. 1. CID MS/MS of the precursor ions: $[M+H]^+$ at *m/z* 379 (A); $[M+Na]^+$ at *m/z* 401 (B); $[2M+H]^+$ at *m/z* 757 (C), and $[2M+Na]^+$ at *m/z* 779 (D).

Table 2
CID MS/MS of the $[M+H]^+$ ion at *m/z* 379

Compounds		CE = 20 V			CE = 30 V			CE = 40 V		
	m/z	379	253	131	379	253	131	379	253	131
(1′*R*,3′*S*),(1′*S*,3′*S*) **1**	%	10.1	24	100	9.1	22	100	8.1	20	100
(1′*R*,3′*R*),(1′*S*,3′*R*) **2**	%	11.2	25	100	9.0	23	100	8.2	20	100

obtained from various low-energy tandem mass spectrometric analyses of the diagnostic fragment ions produced by the various precursor molecules. We have opted to use ESIMS, since this is, arguably, one of the softest ionization methods and which requires neither derivatization nor excessive manipulation of the analytes. As shown by Fenn and co-workers,[26] electrospray ionization is a well established and robust technique for use with combined liquid chromatography–mass spectrometry (LC–MS) which allows rapid and sensitive analysis of a wide range of analyzed compounds, from low molecular-mass polar compounds (<200 Da) to biopolymers (>1000 kDa).

2. Results and discussion

The ESIMS (positive-ion mode) of the anomeric mixture (1′*R*,3′*S*), (1′*S*,3′*S*) **1** and (1′*R*,3′*R*), (1′*S*,3′*R*), **2** of 1-(3-benzoyloxymethyl-1,3-dihydrobenzo[*c*]furan-1-yl)-thymine were recorded with a cone voltage of 20 V and are summarized in Table 1. The ESIMS of **1** showed abundant protonated molecules $[M+H]^+$ at *m/z* 379, as well as high intensities for the sodium complex molecule $[M+Na]^+$ at *m/z* 401. It also contained the protonated dimeric and sodium complex adduct ion clusters corresponding to the $[2M+Na]^+$ and $[2M+H]^+$ at *m/z* 779 and 754. One of the most abundant fragment-ions was obtained by cleavage of the base–glycone C–N bond (pseudo-S-type cleavage), to afford the base-peak ion $[S-C_6H_5CO_2H]^+$ at *m/z* 131.

To investigate the origins of formation of the two fragment ions at *m/z* 253 and 131, low-energy CID MS/MS were obtained separately for the selected $[M+H]^+$, $[M+Na]^+$, $[2M+H]^+$ and $[2M+Na]^+$ molecular species at *m/z* 379, 401, 754 and 779, respectively, observed in the conventional ESIMS of **1** and **2**. Low-energy CID MS/MS is a valuable method for generating structural information, especially if the primary ionization does not impart enough internal energy for spontaneous fragmentation to occur.[27–29] In this process, a portion of the kinetic energy of the ion is converted into internal energy by collision with a neutral gas-phase species, usually in the pressurized collision cell of a tandem mass spectrometer[27–29] and the ions that have undergone collisional excitation may subsequently fragment.

The product-ion spectrum arising from the fragmentation of the selected protonated molecule $[M+H]^+$ at *m/z* 379 derived from **1** in the RF-only hexapole collision cell is presented in Fig. 1(A). The tandem mass spectrum of the ion at *m/z* 379 suggests the formation of the glycone oxonium ion $[S]^+$ at *m/z* 253 and its elimination product ion $[S-C_6H_5CO_2H]^+$ at *m/z* 131. The tandem mass spectra of the protonated molecule $[M+H]^+$ at *m/z* 379, obtained from the diastereomeric and anomeric thymine nucleoside analogues **1** and **2**, respectively, using different collision energies, are summarized in Table 2. The precursor-ion scan of the $[S-C_6H_5CO_2H]^+$ ion at *m/z* 131 indicates that this ion can be formed directly from the protonated molecule $[M+H]^+$ by concerted elimination of separate molecules of the nucleobase and benzoic acid. It can also originate from a stepwise elimination from the glycone oxonium ion $[S]^+$ at *m/z* 253 followed by elimination of a molecule of benzoic acid. Similarly, this precursor ion

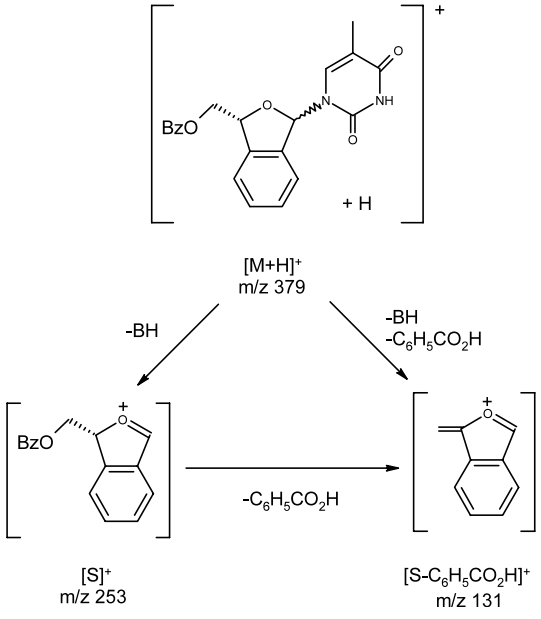

Fig. 2. Proposed fragmentation routes of the protonated molecule $[M+H]^+$ for the (1′*R*,3′*R*),(1′*S*,3′*R*)-thymine analogue **2**.

Table 3
CID MS/MS of the $[2M+H]^+$ ion at *m/z* 757

Compounds		CE = 20 V				CE = 30 V				CE = 40 V				CE = 50 V			
	m/z	757	379	253	131	757	379	253	131	757	379	253	131	757	379	253	131
(1′*R*,3′*S*),(1′*S*,3′*S*) **1**	%	11.8	34.2	71	100	8.5	72	100	50	4.1	33	94	100	3	15	43	100
(1′*R*,3′*R*),(1′*S*,3′*R* **2**	%	12.4	36.7	71	100	9	70	100	51	4.2	36	88	100	3.3	13	45	100

originates from the $[M+Na]^+$, $[2M+H]^+$ and $[2M+Na]^+$ parent ions.

Interestingly, in this series of CID MS/MS, the complete absence of the expected $[BH_2]^+$ ion, contrasts with the expected behavior for common nucleosides (see Fig. 1(A)). The fragmentation route for the product-ion spectra of the $[M+H]^+$ ion has been rationalized using the systematic nomenclature for nucleoside fragmentation in FAB MS proposed by Crow et al.[29] In this proposed fragmentation pathway, the ''main'' fragment-ion $[BH_2]^+$ formation appears to be initiated by an intramolecular transfer of a hydrogen atom from the sugar moiety to the base, which is already protonated. The only other ion produced is usually the less abundant fragment ion $[S]^+$ obtained by cleavage of the glycosidic bond with charge retention on the sugar moiety.[14–16,29]

The proposed fragmentation routes of the $[M+H]^+$ ion at *m/z* 379 from **1**, observed during the CID MS/MS experiment, are tentatively presented in Fig. 2. The connectivities between the fragment ions were also confirmed using additional precursor ion scans of the glycone oxonium ion $[S]^+$ at *m/z* 253 and of the $[S-C_6H_5CO_2H]^+$ ion at *m/z* 131, which indicated that they were both formed from the $[M+H]^+$ ion.

The tandem mass spectra, recorded with different collision energies, of the protonated dimeric cluster $[2M+H]^+$ at *m/z* 757, originating from the anomeric mixtures of nucleosides **1** and **2**, are summarized in Table 3. The latter suggests the formation of the protonated molecule $[M+H]^+$ at *m/z* 379, the glycone oxonium ion $[S]^+$ at *m/z* 253 and the fragment ion $[S-C_6H_5CO_2H]^+$ at *m/z* 131 base peak (Fig. 1(C)).

Inspection of Tables 2 and 3 shows that there are no pronounced differences in the intensities of all the product ions obtained with different collision energies. This is not surprising, as the anomeric mixtures (1′*S*,3′*S*), (1′*R*,3′S) **1** and (1′*S*,3′*R*), (1′*R*,3′*R*) **2** are indeed 1:1 mixtures and also mirror images and, as such, no differences would be expected for the CID MS/MS of the $[M+H]^+$ and $[2M+H]^+$ ions at *m/z* 379 and 757, respectively.

The tandem mass spectra of the sodium complex molecule $[M+Na]^+$ at *m/z* 401, selected individually from the respective anomeric mixture of nucleoside analogues **1** and **2**, are summarized in Table 4 and presented in Fig. 1(B). Interestingly, the product-ion scan of *m/z* 401 shows the presence of the protonated–sodiated thymidine base $[BH+Na]^+$ ion at *m/z* 149 and the fragment ion $[S-C_6H_5CO_2H]^+$ at *m/z* 131. Furthermore, we note the total absence of the glycone oxonium ion $[S]^+$ at *m/z* 253. This is because, most probably, during this CID MS/MS, there is indeed a transfer of a proton from the glycone portion to the sodiated nucleobase to afford the $[BH+Na]^+$ ion at *m/z* 149 and when this process occurs it precludes the formation of the glycone oxonium ion $[S]^+$ at *m/z* 253.

Table 4
CID MS/MS of the $[M+Na]^+$ ion at m/z 401

Compounds		CE = 20 V			CE = 30 V			CE = 40 V		
	m/z	401	149	131	401	149	131	401	149	131
(1′*R*,3′*S*),(1′*S*,3′*S*) **1**	%	100	5	4	39.2	58	100	29.1	61	100
(1′*R*,3′*R*),(1′*S*,3′*R* **2**	%	100	10	11	41.3	43	100	30.2	49	100

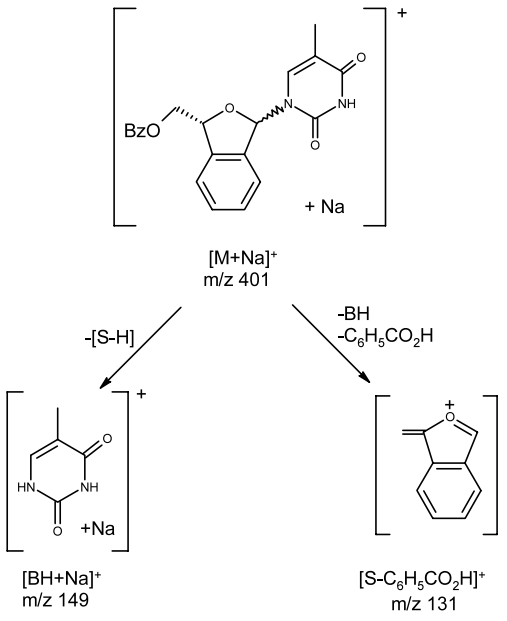

Fig. 3. Proposed fragmentation routes of the sodiated molecule $[M+Na]^+$ for the (1′*R*,3′*R*),(1′*S*,3′*R*)-thymine analogue **2**.

The precursor-ion scan of the $[S-C_6H_5CO_2H]^+$ ion at m/z 131 indicates that, in this case, it originates directly from the selected precursor sodium complex $[M+Na]^+$ molecule and not by elimination of a molecule of benzoic acid from the glycone oxonium ion $[S]^+$. Therefore, we can postulate that, in the tandem mass spectrum of the sodium complex molecule $[M+Na]^+$ at m/z 401, we have two concerted cleavages which occur simultaneously; the formation of the $[BH+Na]^+$ ion at m/z 149, which may occur by proton transfer of either H′-3 or by H′-5/H″-5, and the simultaneous formation of the $[S-C_6H_5CO_2H]^+$ ion at m/z 131 which occurs by elimination of a molecule of benzoic acid. Since we did not have any deuterated labeled compounds, the exact location of the proton elimination was not investigated further.

It is noteworthy that, in contrast to the CID MS/MS of the protonated molecule $[M+H]^+$ at m/z 379 and the dimeric protonated cluster $[2M+H]^+$ at m/z 757, there is a pronounced difference in the intensities of the product ions obtained from CID MS/MS of the $[M+Na]^+$ ion at m/z 401 for **1** as compared to **2**. This is probably due to the difference in the structures or pathways of dissociation of the $[M+Na]^+$ ions obtained from **1** and **2** during the CID MS/MS experiment. That is to say, for each population of $[M+Na]^+$ ions, we can have different affinities for the sodium ion by each of the different positional sites of the electron donating N-1 and N-3, and the carbonyl C-2 and C-4 heteroatoms located on the individual nucleobase which are susceptible to cationization. This may result in different pathways of dissociation, hence reflecting the differences in the intensities of the $[BH+Na]^+$ ion at m/z 149, observed for the various collision energies used during the CID MS/MS. The proposed fragmentation routes of the product-ion spectrum of the $[M+Na]^+$ ion are presented in Fig. 3. Similar results were also noted during the CID MS/MS of the dimeric sodium complex cluster. The tandem mass spectra of the sodium complex cluster $[2M+Na]^+$ at m/z 779, selected individually from **1** and **2**, were recorded with different collision energies and are presented in Table 5 (Fig. 1(D)). The product-ion scan of the ion at m/z 779 indicates the formation of the sodium complex molecule $[M+Na]^+$ at m/z 401, the sodiated–protonated base $[BH+Na]^+$ ion at m/z 149, and the fragment ion $[S-C_6H_5CO_2H]^+$ at m/z 131. The data in Table 4 indicate that, with a collision energy of 40 V for the CID MS/MS experiment, we could observe discriminating fingerprints,

Table 5
CID MS/MS of the $[2M+Na]^+$ ion at m/z 779

Compounds		CE = 20 V				CE = 30 V				CE = 40 V			
	m/z	779	401	149	131	779	401	149	131	779	401	149	131
(1′*R*,3′*S*),(1′*S*,3′*S*) **1**	%	7.3	100			7	100	5	9	5.1	100	27	33
(1′*R*,3′*R*),(1′*S*,3′*R*) **2**	%	7.2	100			6.8	100	6	7	4.3	92	46	100

Table 6
Electrospray mass spectra of enantiomeric and diastereomeric pairs of *cis*- and *trans*-1-(3-benzoyloxymethyl-1,3-dihydrobenzo[*c*]furan1-yl)-uracils (**3**–**6**) recorded with a cone voltage of 20 V

Compounds		Characteristic ions						
		$[2M+Na]^+$	$[2M+H]^+$	$[2M+H\text{-}BH\text{-}C_6H_5CO_2H]^+$	$[M+Na]^+$	$[M+H]^+$	$[S]^+$	$[S-C_6H_5CO_2H]^+$
	m/z	751	729	495	387	365	253	131
(1′*S*,3′*R*) **3**	%	8.8	9.5	9.4	12.3	52.3	100	100
(1′*R*,3′*S*) **4**	%	9.4	10.1	2.9	20.1	15.3	54.1	100
(1′*R*/3′*R*) **5**	%	9.4	26.4	2.9	14.1	15.2	56.4	100
(1′*S*/3′*S*) **6**	%	9.1	22.3	—	19	18.2	95.2	100

indicating inequalities of chemical free energy and sodiation affinity sites on the individual base, which is reflected in the intensities of the product ions obtained from the different pathways of dissociation of the precursor ions.

The ESIMS (positive-ion mode) of the enantiomeric pairs of *cis*- and *trans*-(3-benzoyloxymethyl-1,3-dihydrobenzene[*c*]furan-1-yl)uracil (**3**–**6**) were recorded with a cone voltage of 20 V and are summarized in Table 6. The ESIMS of this set of two enantiomeric pairs gave a similar pattern of protonated and sodium complex molecules, cluster of dimers and fragment ions, as already observed for the thymine nucleoside analogues **1** and **2** indicated in Table 2. The absence of the $[BH_2]^+$ and $[BH+Na]^+$ ions at *m/z* 113 and *m/z* 135, respectively, is notable. We observed the presence of the diagnostic ion at *m/z* 495, which seems to originate from the protonated dimeric adduct cluster, and this formation is rationalized by the losses of the uracil base and benzoic acid molecules and, as such, was assigned as the $[2M+H-BH-C_6H_5CO_2H]^+$ ion.

Low-energy CID MS/MS analyses were conducted with different collision energies on the protonated molecule $[M+H]^+$ and protonated dimeric cluster $[2M+H]^+$ at *m/z* 365 and 729, respectively and are presented in Tables 7 and 8. The tandem mass spectra of the $[M+H]^+$ ion at *m/z* 365 confirms the formation of the glycone oxonium ion $[S]^+$ at *m/z* 253 and its elimination product ion $[S-C_6H_5CO_2H]^+$ at *m/z* 131. The absence of the $[BH_2]^+$ ion at *m/z* 113 is once more noted. The data in Table 7 indicate that there are essentially no discriminating or major changes in the intensities of the product ions obtained within a corresponding enantiomeric or diastereomeric pair. This is not surprising, and was obviously expected as each pair **3**, **4**, and **5**, **6** are, indeed, mirror images and, as such, we anticipated that the tandem mass spectra ion fragmentations would be identical. Note that any changes in intensity of the product ions by a difference of 2–3% were arbitrarily assigned as "no change."

The tandem mass spectrum of the dimeric protonated cluster $[2M+H]^+$ ion at *m/z* 729 indicated the formation of the protonated molecule at *m/z* 365, the glycone oxonium ion $[S]^+$, and the $[S-C_6H_5CO_2H]^+$ ions at *m/z* 253 and 131, respectively. It also confirmed the genesis of the $[2M+H-BH-C_6H_5CO_2H]^+$ ion at *m/z* 495 as originating from the $[2M+H]^+$ ion (see Fig. 4).

In contrast to the tandem mass spectra of the $[2M+H]^+$ ions obtained for **1** and **2**, the CID MS/MS of the $[2M+H]^+$ ion at *m/z* 729, recorded with different collision energies, indicated that there were noticeable differences in the intensities of some of the product ions obtained within each enantiomeric and diastereomeric pair (Fig. 4). Perhaps this is not surprising since, in each enantiomeric or diastereomeric species, selected precursor ions are composed of clusters of species formed by two identical nucleosides which, in gas phase and during the MS/MS experiment, possess the same chemical free energy of activation and stereoelectronic environment. This, perhaps, restricts the protonation of either one or two of the N-1 and N-3 heteroatoms which leads to the formation of isomeric populations of the $[2M+H]^+$ ion tertiary structures. It is noteworthy that, during an MS/MS experiment, the dissociation of the selected precursor ion (also called the parent ion) generates product ions with different kinetic energy and momenta from the parent ion.[27] This causes the differences in the intensities of identical product ions for different collision energies used in the MS/MS experiment. On the other hand, when one deals with a 1:1 anomeric mixture, as in the MS/MS of the $[2M+H]^+$ ions selected from **1** and **2**, this type of tertiary structure of the cluster ions becomes more complex. Thus, the probability of protonation of the different electronegative sites increases and results in formation of a larger population of isomeric ion-clusters. This results in product ions with no distinct differences in their respective intensities.

The tandem mass spectra of the sodium complex molecule $[M+Na]^+$ at *m/z* 387 were recorded with different collision energies and are presented in Table 9. As shown earlier in the case of the thymine nucleoside analogues **1** and **2**, we observed the formation of the $[BH+Na]^+$ ion at *m/z* 135 and the $[S-C_6H_5CO_2H]^+$ ion at *m/z* 131. The absence of the glycone oxonium ion

Table 7
CID MS/MS of the $[M+H]^+$ ion at *m/z* 365

Compounds		CE = 10 V			CE = 20 V			CE = 30 V			CE = 40 V			CE = 50 V		
	m/z	365	253	131	365	253	131	365	253	131	365	253	131	365	253	131
(1′*S*,3′*R*) **3**	%	38.8	100	20	11	38.8	100	8.4	19	100	5.8	12	100	5.0	10	100
(1′*R*,3′*S*) **4**	%	37.6	100	21	12.3	38..5	100	8.2	18.6	100	5.0	11.1	100	4	11	100
(1′*R*/3′*R*) **5**	%	32	100	28.8	11.2	29.4	100	7	17.1	100	4.0	11	100	3.0	7.0	100
(1′*S*/3′*S*) **6**	%	32.5	100	28.5	11	30.2	100	8	19	100	5.2	11.7	100	5.1	9	100

Table 8
CID MS/MS of the $[2M+H]^+$ ion at *m/z* 729

Compounds		CE = 10 V					CE = 20 V					CE = 30 V					CE = 40 V					CE = 50 V				
	m/z	729	495	365	253	131	729	495	365	253	131	729	495	365	253	131	729	495	365	253	131	729	495	365	253	131
(1′*S*,3′*R*) **3**	%	100	5	33	31	8	21.1	2.7	47	100	19	22.3	2.1	43	100	67	5.8		15	59	100	2.4		7	41	100
(1′*R*,3′*S*) **4**	%	100	2.5	32.3	31	6.4	14.7	1.7	34.1	100	15.8	20.0	1.1	37.6	100	73	7		11	54.1	100	1.7		5.2	37	100
(1′*R*/3′*R*) **5**	%	100	5.2	34.1	45.3	11.7	15.2	1.7	30	100	27	10.0	1.1	28.8	100	95.2	4		7.6	42.3	100	1		3.5	28.2	100
(1′*S*/3′*S*) **6**	%	100	5	43	47	11	12.9	1.7	36	100	21	14.1	1.7	33	100	78	4.2		10	51	100	1.1		4.1	35	100

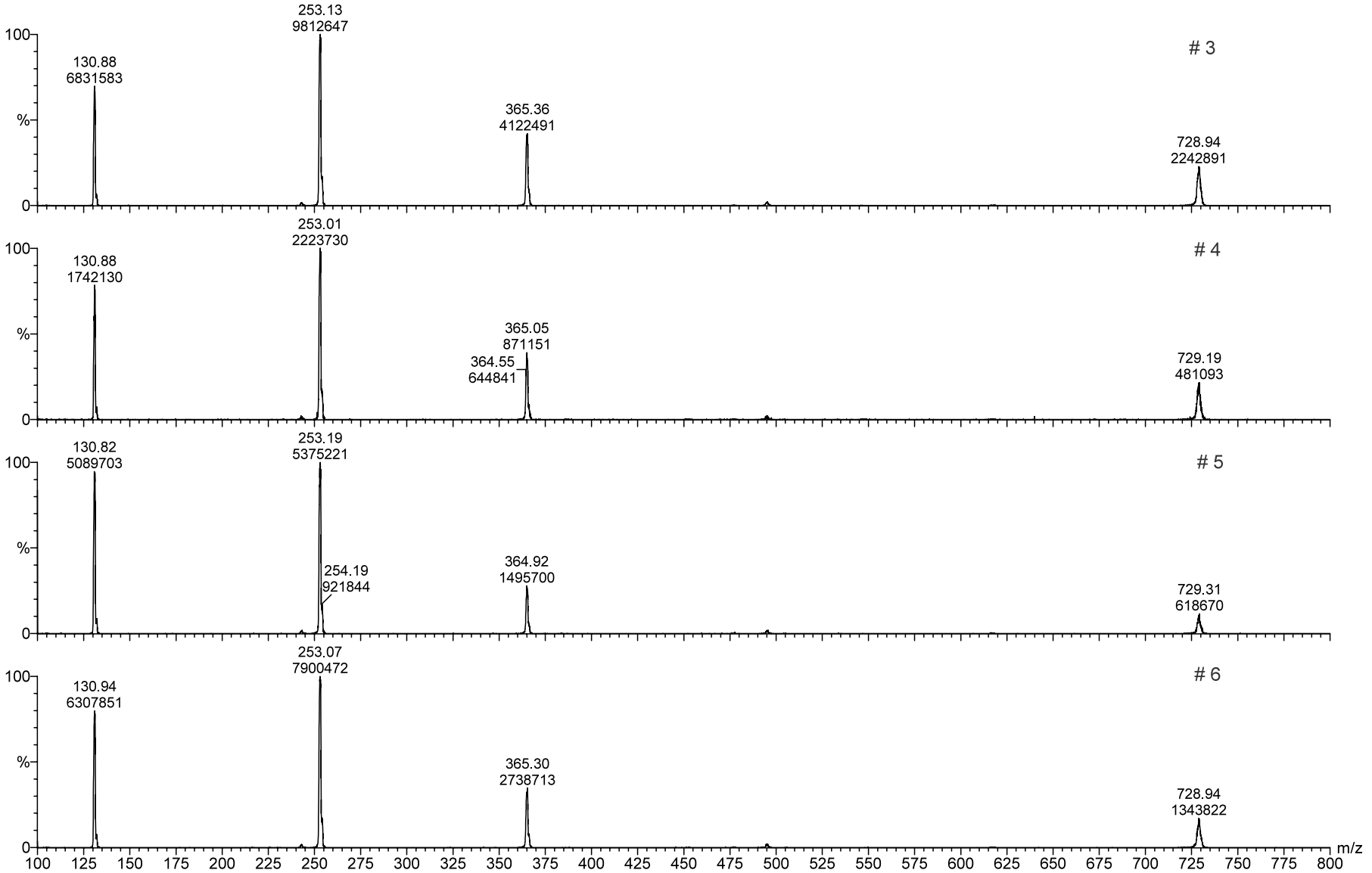

Fig. 4. CID MS/MS of the $[2M+H]^+$ ion at *m/z* 729 obtained for the pure enantiomers **3**–**6** with a collision energy of 30 V.

Table 9
CID MS/MS of the $[M+Na]^+$ ion at *m/z* 387

Compounds		CE = 10 V			CE = 20 V			CE = 30 V			CE = 40 V			CE = 50 V		
	m/z	387	135	131	387	135	131	387	135	131	387	135	131	387	135	131
(1′*S*,3′*R*) **3**	%	100	4.7	1.1	100	24.7	13.8	100	100	91.7	63.5	81.7	100	47	69.4	100
(1′*R*,3′*S*) **4**	%	100	10	–	100	27.7	16.4	92.9	100	91.1	62.1	82.3	100	60	54.2	100
(1′*R*/3′*R*) **5**	%	100	4.1	2.9	100	22.9	18.8	73.5	86.4	100	44.1	62.9	100	34.1	54.1	100
(1′*S*/3′*S*) **6**	%	100	2.9	1.1	100	17	14.7	100	84.1	100	70	66.4	100	47	55.2	100

$[S]^+$ was also noted. The CID MS/MS of the enantiomeric pair **3** to **6** showed pronounced differences in the intensities of the product ions, especially for those recorded with collision energies of 10, 20, and 50 V (Fig. 5).

Finally, the CID MS/MS of the dimeric sodium complex cluster $[2M+Na]^+$ at *m/z* 751 were recorded and are presented in Table 10. The tandem mass spectra indicated the formation of the sodium complex molecule $[M+Na]^+$ at *m/z* 387. The $[BH+Na]^+$ and $[S-C_6H_5CO_2H]^+$ ions at *m/z* 135 and 131, respectively, were also formed (Fig. 6). Once more, in this MS/MS analysis, we can observe differences in the intensities of the product ions formed. For the enantiomers **3** and **4**, the only difference in intensities was noted in the CID MS/MS recorded with a collision energy of 10 V, whereas, in the case of enantiomers **5** and **6**, discriminating differences were noted for all of the different collision energies used.

For more confirmatory evidence on the genesis of the $[BH+Na]^+$ product ion, an MS/MS precursor ion scan of the ion at *m/z* 135 was recorded and showed that it was formed from the $[M+Na]^+$ and $[2M+Na]^+$ adducts at *m/z* 387 and 751, respectively. Similarly, the precursor-ion scan of the $[S-C_6H_5CO_2H]^+$ ion at *m/z* 131 showed that it was formed from all of the precursor molecular ion species and/or the glycone oxonium ion $[S]^+$ at *m/z* 253.

The aim of this study was to establish the fragmentation routes of two sets of diastereomeric nucleoside analogues **1** and **2**, and the four enantiomers of the analogous uracil nucleosides **3**–**6** by electrospray mass spectrometry. This investigation demonstrates that this technique facilitates the characterization of the proposed structures. Assignment of core structures was based mainly on the interpretation of product-ion spectra of selected precursor ions. In addition, MS/MS, using low-energy collisional activation of singly protonated and sodium complex precursor ions, provided characteristic fingerprints which allowed the proper identification of the anomeric mixture (1:1) of the thymine analogues and the pure enantiomers of the uracil analogues. For the $[2M+Na]^+$, $[2M+H]^+$, and $[M+Na]^+$ precursor ions at *m/z* 751, 729, and 387, respectively, obtained from the pure enantiomeric pairs **3** and **4**, and **5** and **6**, discriminating fingerprint ion intensities showed differences with each enantiomeric pair. However, in the tandem mass spectra obtained for the precursor ion $[M+H]^+$ at *m/z* 365, the difference between the product ion intensities within each enantiomeric pair were, as expected, not significant. The fingerprint ion intensity reflects the inequalities of the chemical free energy and the differences of the proton and sodium complexation on different stereochemical sites of the nucleobase, which contributes to the differences in the tertiary structure of the precursor molecular ions.

3. Experimental

3.1. Sample preparation

The two anomeric pairs of the diastereoisomeric *cis*- and *trans*-1-(3-benzoyloxymethyl-1,3-dihydrobenzo[*c*]furan-1-yl)thymines **1** and **2**, and the pure enantiomers of *cis*- and *trans*-1-(3-benzoyloxymethyl-1,3-dihydrobenzo[*c*]furan-1-yl)uracil, (1′*S*,3′*R*)- **3**, (1′*R*, 3′*S*)- **4**, (1′*R*, 3′*R*)- **5** and (1′*S*,3′*S*)- **6**, were obtained as reported elsewhere.[8–11] The standard solutions used for LC/MS and LC/MS/MS were prepared with a mixture of HPLC solvent-grade methanol–water (CH_3OH-H_2O, 50:50) at a concentration of 50 pmol μL^{-1}. A 20-μL aliquot of sample was then introduced into the electrospray ion source by a continuous flow of (CH_3OH-H_2O, 50:50) at a flow rate of 10 μL min^{-1} using a Shimadzu LC-10AD pump connected to a Rheodyne injector with a 20 μL loop.

3.2. Mass-spectrometric conditions

The ESI mass spectra (positive-ion mode) were recorded with a Micromass Quattro quadrupole–hexapole–quadrupole mass spectrometer equipped with a mega-flow ESI source and capable of analyzing ions up to *m/z* 4000. A personal computer (Compaq, PIII 300 MHz processor, running Windows NT 4, service pack 3) equipped with Micromass MASSLYNX 3.3 Mass

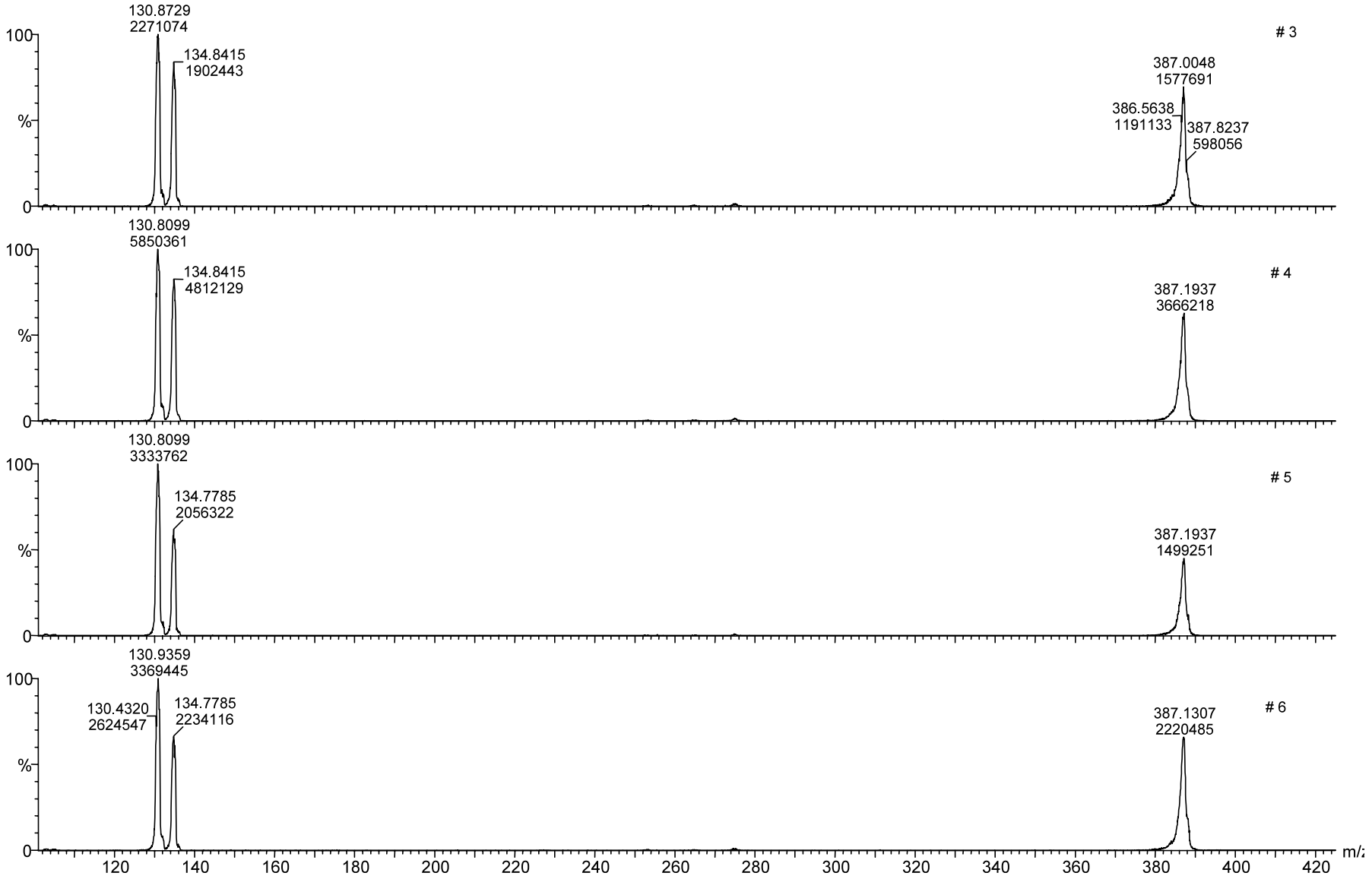

Fig. 5. CID MS/MS of the $[M+Na]^+$ ion at *m/z* 387 obtained for the pure enantiomers **3**–**6** with a collision energy of 50 V.

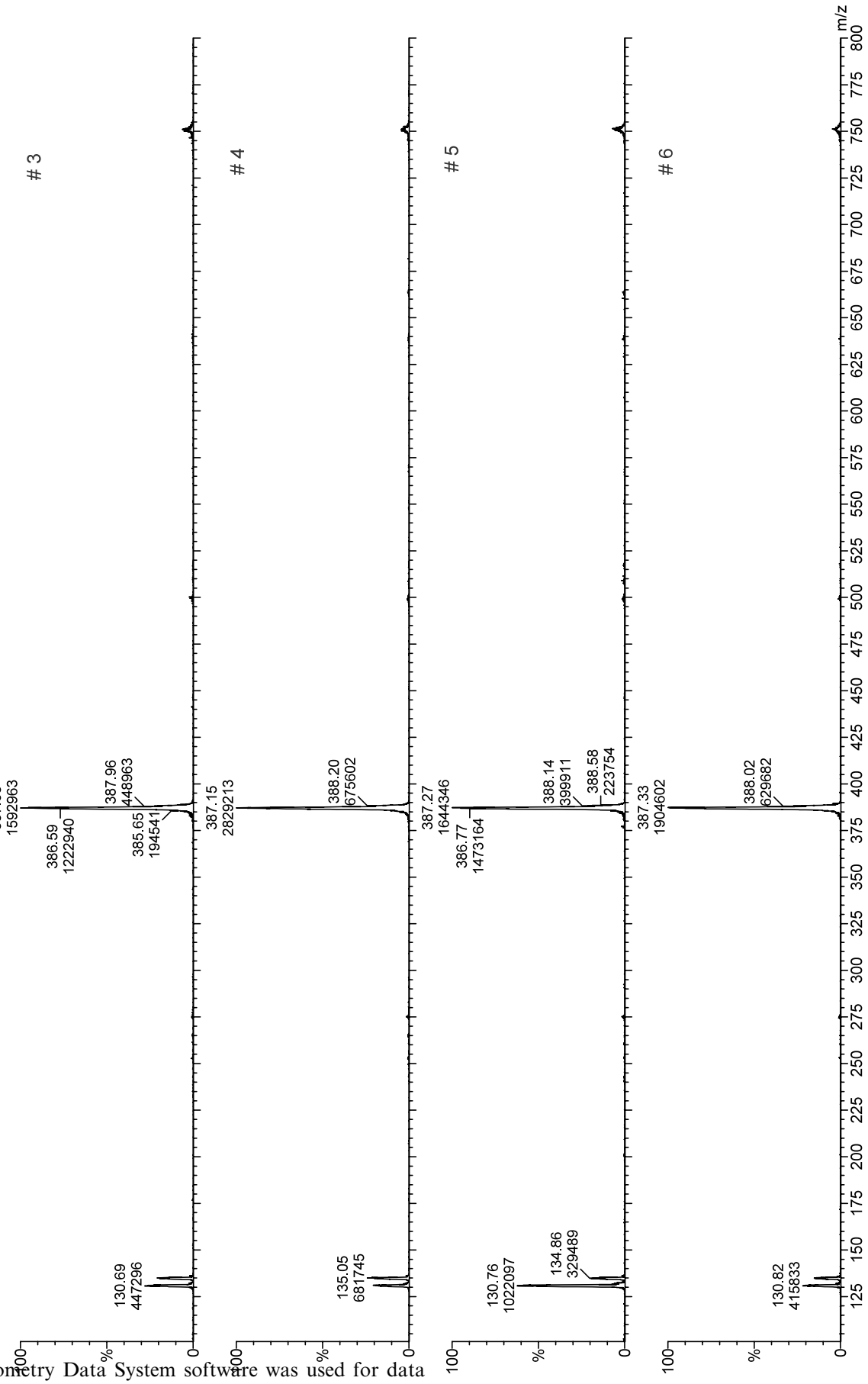

Fig. 6. CID MS/MS of the $[2M+Na]^+$ ion at *m/z* 756 obtained for the pure enantiomers **3**–**6** with a collision energy of 50 V.

Spectrometry Data System software was used for data

Table 10
CID MS/MS of the $[2M+Na]^+$ ion at *m/z* 751

Compounds		CE = 10 V				CE = 20 V				CE = 30 V				CE = 40 V				CE = 50 V			
	m/z	751	387	135	131	751	387	135	131	751	387	135	131	751	387	135	131	751	387	135	131
(1′*S*,3′*R*) **3**	%	100	69			21	100			15.8	100	1	4	8.8	100	4	8	4.1	100	17	27
(1′*R*,3′*S*) **4**	%	84.4	100			18.8	100		1.0	10	100	2	1	8.2	100	5.8	6.4	2.9	100	22.3	20
(1′*R*/3′*R*) **5**	%	100	88.2			25.8	100		4.7	11.4	100		7.8	11.7	100	4.7	22.3	5.8	100	21.7	65.8
(1′*S*/3′*S*) **6**	%	100	81			21	100			8.2	100		1	7.8	100	3	6	3.5	100	14	21

acquisition and processing. The temperature of the ESI source was maintained at 75 °C. The operating voltage of the ESI capillary was 3.00 kV and the high-voltage lens was set at 0.40 kV throughout the whole operation. ESIMS were recorded with a cone voltage of 25 V. Conventional ESI mass spectra were obtained by scanning in the Multi Channel Analysis mode (MCA) with a scan time of 1 s per 250 mass numbers. Spectra are an average of 20–30 scans. The mass scale was calibrated in the positive-ion mode using a polyethylene glycol mixture. Component analysis of ESIMS was performed using MASSLYNX algorithms which converts a range of multiply charged cations into identifiable single components. ESIMS with "maximum entropy" (ESIMS-MaxEnt) was performed using the Micromass MaxEnt Deconvolution (MMD) program. MaxEnt automatically disentangles the *m/z* spectrum produced by the mass spectrometer and presents the data for each individual 1,3-dihydrobenzo[*c*]furan nucleoside analogue in a single peak on a true molecular weight scale. Product ion MS/MS experiments were conducted using the same instrument. Product-ion spectra of mass-selected precursor molecular-ion species were induced by collision with argon in the (r.f.-only) hexapole. The resulting fragment ions were analyzed by the second quadrupole. CID tandem mass spectra were recorded in an MCA mode and are consistently a combined average of 25 scans for each type of precursor ion. A cone voltage varying from 20 to 35 V, collision energies varying from 10 to 40 eV and a collision gas pressure in the collision cell varying from 3.5×10^{-4} to 6.5×10^{-4} mbar (1 bar = 10^5 Pa) were used in all MS/MS experiments. The collision gas pressure was increased to induce the dissociation of the sodiated adduct anions (typical settings were around 6.0×10^{-4} mbar). Precursor-ion MS/MS scans were obtained by scanning the first quadrupole while selecting a given *m/z* value with the second quadrupole.

Acknowledgements

Joseph Banoub acknowledges the Natural Sciences and Engineering Research Council of Canada for financial support in the form of a Discovery Grant.

References

1. Mitsuya, H.; Weinhol, K. J.; Furman, P. A.; St Clair, M. H.; Nusinoff-Lejrman, S.; Gallo, R. C.; Bolognesi, D. P.; Barry, D. W.; Broder, S. *Proc. Natl. Acad. Sci. USA* **1985**, *82*, 7096–7100.
2. Cooney, D. A.; Dalal, M.; Mitsuya, H.; McMahon, J. B.; Nadkarni, M.; Balzarini, J.; Broder, S.; Johns, D. G. *Biochem. Pharmacol.* **1986**, *35*, 2065–2068.

3. Ahluwalia, G.; Cooney, D. A.; Mitsuya, H.; Fridland, A.; Flora, K. P.; Hao, Z.; Dalal, M.; Broder, S.; Johns, D. G. *Biochem. Pharmacol.* **1986**, *35*, 3797–3800.
4. Coates, J. A.; Cammack, N. S.; Jenkinson, H. J.; Jowett, M. I.; Pearson, B. A.; Pen, C. R.; Rouse, P. L.; Viner, K. C.; Cameron, J. M. *Antimicrob. Agents Chemother.* **1992**, *36*, 733–739.
5. Balzarini, J.; Kang, C. J.; Dalal, M.; Herdewijn, P.; De Clercq, E.; Broder, S.; Johns, D. G. *Mol. Pharmacol.* **1987**, *32*, 162–167.
6. Lea, A. P.; Faulds, D. *Drugs* **1996**, *51*, 846–864.
7. Simpson, M. V.; Chin, C. D.; Keilbaugh, S. A.; Lin, T. S.; Prusoff, W. H. *Biochem. Pharmacol.* **1989**, *38*, 1033–1036.
8. Ewing, D. F.; Fahmi, N.; Len, C.; Mackenzie, G.; Ronco, G.; Villa, P.; Shaw, G. *Collect. Czech. Chem. Commun.* **1996**, *61*, S145–S146.
9. Ewing, D. F.; Fahmi, N.; Len, C.; Mackenzie, G.; Ronco, G.; Villa, P.; Shaw, G. *Nucleosides Nucleotides* **1999**, *18*, 2613–2630.
10. Ewing, D. F.; Fahmi, N.; Len, C.; Mackenzie, G.; Pranzo, A. *J. Chem. Soc. Perkin Trans. I* **2000**, *21*, 3561–3565.
11. Ewing, D. F.; Len, C.; Mackenzie, G.; Ronco, G.; Villa, P. *Tetrahedron: Asymmetry* **2000**, *11*, 4995–5002.
12. Humble, R. W.; Mackenzie, G.; Shaw, G. *Nucleosides Nucleotides* **1984**, *3*, 363–367.
13. Russ, P. L.; Hegedus, L.; Kelly, J. A.; Barchi, J. J.; Marquez, V. E. *Nucleosides Nucleotides* **1992**, *11*, 351.
14. Banoub, J.; Mackenzie, G.; Descotes, G.; Humble, R. W.; Shaw, G.; Becchi, M.; Fraisse, D. *Biomed. Environ. Mass Spectrom.* **1990**, *19*, 97–99.
15. Banoub, J.; Becchi, M.; Descotes, G.; Fraisse, D.; Humble, R. W.; Mackenzie, G. *J. Carbohydr. Chem.* **1992**, *11* (4), 471–484.
16. Banoub, J.; Gentil, E.; Tber, B.; Fahmi, N. E.; Ronco, G.; Villa, P.; Mackenzie, G. *Spectroscopy Int. J.* **1994**, *12*, 69–83.
17. Chauvin, C.; Thibault, P.; Plusquellec, D.; Banoub, J. *J. Carbohydr. Chem.* **1993**, *12*, 459–475.
18. Baczko, C.; Nugier-Chauvin, C.; Banoub, J.; Thibault, P.; Plusquellec, D. *Carbohydr. Res.* **1995**, *269*, 79.
19. Gentil, E.; Lesimple, A.; Le Bigot, Y.; Delmas, M.; Banoub, J. *Rapid Commun. Mass Spectrom.* **1994**, *8*, 869–875.
20. Banoub, J.; Becchi, M.; Lafont, D.; Descotes, G.; Fraisse, D. *Rapid Commun. Mass Spectrom.* **1990**, *4*, 536–540.
21. Helleur, R. J.; Thibault, P.; Shaw, D. H.; Banoub, J. *Org. Mass Spectrom.* **1992**, *27*, 967–973.
22. Banoub, J.; Thibault, P.; Goueth, P. Y.; Ronco, G.; Villa, P. *J. Mass Spectrom.* **1997**, *32*, 109–121.
23. Gentil, E.; Banoub, J. *J. Mass Spectrom.* **1996**, *31*, 83–94.
24. Bateman, K. P.; Banoub, J.; Thibault, P. *Electrophoresis* **1996**, *17*, 1818–1828.
25. Banoub, J.; Combden, S.; Miller-Banoub, J.; Sheppard, G.; Hodder, H. *Nucleosides Nucleotides* **1999**, *18* (11&12), 2751–2768.
26. Fenn, J. B.; Mann, M.; Meng, C. K.; Wong, S. F.; Withehouse, C. M. *Science* **1989**, *246*, 64–71.
27. Busch, K. L.; Glish, G. L.; McLuckey, S. *Mass Spectrometry–Mass Spectrometry: Techniques and Applications of Tandem Mass Spectrometry*; VCM Publisher, 1988; p 217.
28. McLafferty, F. W. *Tandem Mass Spectrometry*; Wiley Interscience: New York, 1983; p 532.
29. Crow, F. W.; Tomer, B. K.; Gross, M. L.; McCloskey, J. A.; Bergstrom, D. E. *Anal. Biochem.* **1984**, *139*, 243–262.